J. Plasma Phys. (2023), *vol*. 89, 955890501
Published by Cambridge University Press

doi:10.1017/S0022377823001022

SDR, EVC, and SDREVC: Limitations and Extensions

E.D. Hunter[1,†], C. Amsler[1], H. Breuker[2], M. Bumbar[1], S. Chesnevskaya[1], G. Costantini[3,4], R. Ferragut[5,6], M. Giammarchi[6], A. Gligorova[1], G. Gosta[3,4], H. Higaki[7], C. Killian[1,8], V. Kraxberger[1,9], N. Kuroda[10], A. Lanz[1,9], M. Leali[3,4], G. Maero[6,11], C. Malbrunot[12,‡], V. Mascagna[3,4], Y. Matsuda[10], V. Mäckel[1,§], S. Migliorati[3,4], D.J. Murtagh[1], A. Nanda[1,9], L. Nowak[1,9], F. Parnefjord Gustafsson[1,¶], S. Rheinfrank[1,8], M. Romé[6,11], M.C. Simon[1], M. Tajima[13], V. Toso[5,6], S. Ulmer[2], L. Venturelli[3,4], A. Weiser[1,9], E. Widmann[1], Y. Yamazaki[2] and J. Zmeskal[1]
(The ASACUSA-Cusp Collaboration)

[1]Stefan Meyer Institute for Subatomic Physics, Austrian Academy of Sciences, 1030 Vienna, Austria

[2]Ulmer Fundamental Symmetries Laboratory, RIKEN, 351-0198 Saitama, Japan

[3]Dipartimento di Ingegneria dell'Informazione, Università degli Studi di Brescia, 25121 Brescia, Italy

[4]INFN sez. Pavia, 27100 Pavia, Italy

[5]L-NESS and Department of Physics, Politecnico di Milano, 22100 Como, Italy

[6]INFN sez. Milano, 20133 Milan, Italy

[7]Graduate School of Advanced Science and Engineering, Hiroshima University, 739-8530 Hiroshima, Japan

[8]Faculty of Physics, TU Wien, 1040 Vienna, Austria

[9]University of Vienna, Vienna Doctoral School in Physics, 1090 Vienna, Austria

[10]Institute of Physics, Graduate School of Arts and Sciences, University of Tokyo, 113-8654 Tokyo, Japan

[11]Dipartimento di Fisica, Università degli Studi di Milano, 20133 Milan, Italy

[12]Experimental Physics Department, CERN, 1211 Geneva, Switzerland

[13]RIKEN Nishina Center for Accelerator-Based Science, 351-0198 Saitama, Japan

(Received 5 June 2023; revised 27 August 2023; accepted 29 August 2023)

Methods for reducing the radius, temperature and space charge of a non-neutral plasma are usually reported for conditions which approximate an ideal Penning Malmberg trap. Here, we show that (i) similar methods are still effective under surprisingly adverse circumstances: we perform strong drive regime (SDR) compression and SDREVC in a strong magnetic mirror field using only 3 out of 4 rotating wall petals. In addition, we demonstrate (ii) an alternative to SDREVC, using e-kick instead of evaporative cooling

† Email address for correspondence: eric.david.hunter@cern.ch
‡ Present address: TRIUMF, Vancouver, BC V6T 2A3, Canada
§ Present address: INFICON GmbH, Köln, Germany
¶ Present address: CERN, 1211 Geneva, Switzerland

(EVC) and (iii) an upper limit for how much plasma can be cooled to $T < 20$ K using EVC. This limit depends on the space charge, not on the number of particles or the plasma density.

Key words: plasma properties

1. Introduction

Fine control over plasma parameters is beneficial for experiments that use destructive diagnostics (Hurst *et al.* 2016; Ahmadi *et al.* 2017; Stenson *et al.* 2018), have long cycle times (Amsler *et al.* 2021; Singer *et al.* 2021; Blumer *et al.* 2022) or struggle for limited resources like antimatter (Hori & Walz 2013), rare isotopes (Aumann *et al.* 2022) or highly charged ions (Kluge *et al.* 2008). For many of these experiments, the density n and temperature T of the plasma are key parameters which must be both reproducible, for the reasons just stated, and optimal. In practice, the maximum n and minimum T are far from the theoretical optimum, and it remains an open question whether the observed bounds on n and T are fundamental or merely a sign that better methods are required.

For an electron or positron plasma, n can be continuously tuned using the strong drive regime (SDR) rotating wall technique of Danielson, Surko & O'Neil (2007). The value of T may be reduced via evaporative cooling (EVC) (Andresen *et al.* 2010). When the plasma is cold enough that T is less than its space charge ϕ_0 ($k_B T \ll e\phi_0$, where k_B is Boltzmann's constant and e is the elementary charge), then EVC also reliably defines the latter. Combining these two tools yields a new one, SDREVC, which allows n, ϕ_0, and T to be set simultaneously (Ahmadi *et al.* 2018).

When it works, SDREVC takes as input 'any' plasma (of sufficiently many particles) and produces a user-defined, invariable (to $\sim$1 %) final state – greatly facilitating optimization studies and systematic searches generally. But when does it work? *A priori*, the experimenter cannot give an exhaustive list of the conditions necessary for these techniques to work as advertised. The main ingredient (SDR) is only heuristically described by theory. One must be content to find, empirically, some range of parameters which give good results for a particular trap.

It is useful to know what limits exist and which assumptions are actually relevant to the process. We explore these questions in experiments on electron plasma held in ASACUSA's Cusp Trap (Kuroda *et al.* 2017). Section 2 reviews aspects of the control and diagnostic systems relevant for this work. Each technique is addressed in its own section: SDR in § 3, SDREVC in § 4 and EVC in § 5. Section 6 contains a short discussion of the results, summarizing what can be used for testing a potential theory, and indicating where practical extensions may be possible.

2. Apparatus

We use a Penning Malmberg trap (Malmberg & Driscoll 1980) with inner diameter 34 mm and magnetic field $B \approx 2$ T. The entrance and exit to the trap are screened by copper meshes (geometrical transparency = 79 %) so that microwave radiation from the plasma cannot escape the 6 K cryogenic ultra-high vacuum region (Amsler *et al.* 2022). A typical plasma contains $N \sim 10^7$ electrons, with length $L_p \approx 10$ cm, radius $r_p \approx 1$ mm and $n \sim 10^8$ cm^{-3}. The plasma cools via cyclotron radiation to a steady-state $T \approx 30$ K for $N \lesssim 4 \times 10^7$.

https://doi.org/10.1017/S0022377823001022 Published online by Cambridge University Press

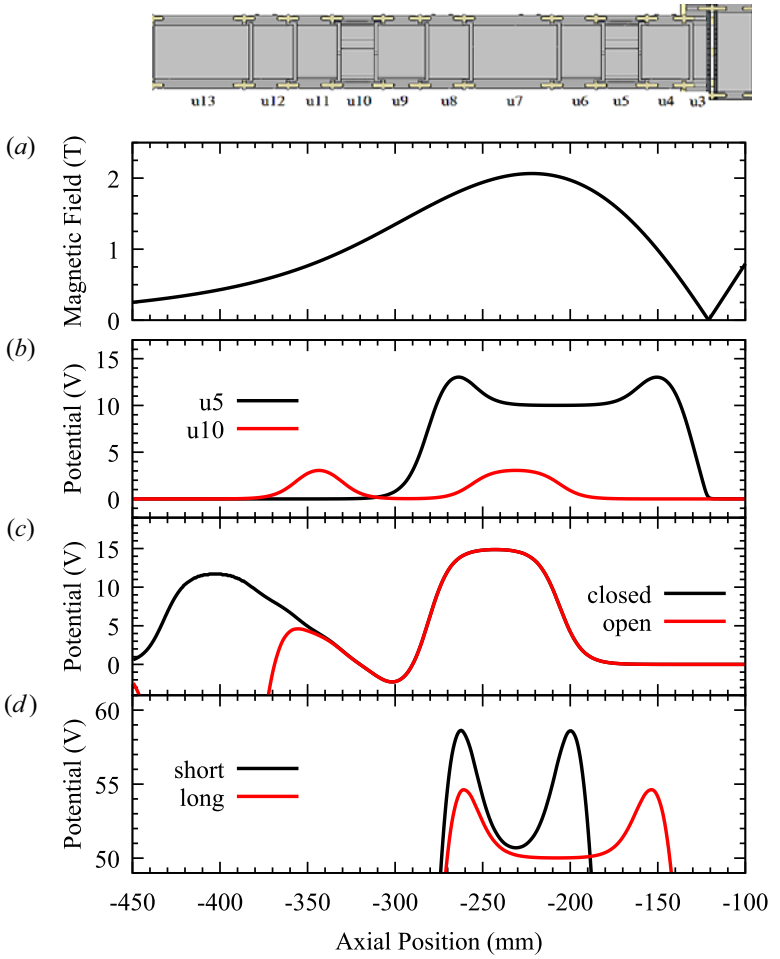

FIGURE 1. Electrode structure and on-axis trapping fields. Two-dimensional rendering of the electrode stack (with electrode names) is shown at the top, followed by (*a*) magnetic field strength B and electrostatic potential for (*b*) standard SDREVC, (*c*) pulsed SDREVC and (*d*) EVC. In this figure the voltages are multiplied by (-1) for clarity; they must be inverted for confining negatively charged particles.

2.1. *Control*

Two pairs of superconducting anti-Helmholtz coils produce B. The axial component of B is shown in figure 1(*a*). The strong gradients were designed to focus low field seeking antiatoms travelling to the right toward the spectroscopy beamline (Nagata & Yamazaki 2014; Nagata *et al.* 2015). Although the coils produce a strong field in three regions, it is difficult to move a plasma into the middle or right region because of the field nulls (cusp points) at ± 120 mm. Plasma is loaded exclusively on the left side, either from an electron source (Nishinbo NJK1120A) or from other traps. Plasma diagnostics (see below) are also performed by dumping to the left.

One electrode, u13, must be pulsed for catching bunches of protons, antiprotons and positrons from those traps (electrode locations are given at the top of figure 1). Two electrodes, u5 and u10, are driven with radiofrequency for SDR and plasma or ion heating.

https://doi.org/10.1017/S0022377823001022 Published online by Cambridge University Press

The other electrodes (u12, u11, u9, u8, u7, u6, u4, u3) have cryogenic 2-pole RC filters mounted as close to the electrode as possible (∼1cm away). These filters attenuate noise with frequency $f > 10$ kHz, which would heat the plasma. The pulsed electrode u13 has a similar filter, but the filter is bypassed by a pair of BAT54 Schottky diodes. The slower, nearly DC bias for the electrodes is supplied by low speed x15 high voltage amplifiers designed by J. Fajans. These amplifiers exhibit excellent stability (approximately 1 mV per year) and noise performance ($0.1\text{mV}_{\text{rms}}$). The price for this performance is a rise time of almost 5ms. This limits the range of plasma dynamics which can be studied in our experiment; for instance, after EVC we must spend 10ms changing the well shape before we can properly diagnose T.

The rotating wall (RW) electrodes u5 and u10 have 4 azimuthal sectors each. Each sector is driven with a sine wave, phase shifted as $\{0^\circ, 90^\circ, 180^\circ, 270^\circ\}$. These signals are produced by the $\{0^\circ, 90^\circ\}$ outputs of a 2-channel arbitrary waveform generator (BK Precision BK4054B) followed by 180° phase splitters (Mini-Circuits ZSCJ-2-2+). The signals then enter a filterbox mounted to the vacuum feedthrough. The filterbox contains a low pass filter for DC biasing of the electrode (RC = 0.2 ms) and high pass filters for the RW signals (RC = 0.01 ms).

One sector of u10 is grounded inside the vacuum chamber (unintentionally); the resistance to ground is less than 4Ω and does not change when the experiment is cooled down. The filter for u10 was modified such that a DC bias could still be applied to two opposing sectors, while the others are 50Ω terminated. A DC bias is applied when dumping the plasma so that the particles leave the trap with at least 10 eV of energy. The bias creates an azimuthal asymmetry, which leads to more rapid plasma expansion (Notte & Fajans 1994). This effect is negligible for short manipulations (10 ms or less). The AC inputs to u10 are essentially the same as for u5's filter. In both cases, the impedance between RW sectors is approximately 50Ω at frequencies above $f \sim 10$ kHz.

A high voltage pulser drives electrode u13 via a similar filter circuit with RC = 0.2 ms. The pulser is similar to the one described by Chaney & Sundararajan (2004), with the addition of a transformer and relay to produce pulses of either polarity.

2.2. *Diagnostics*

To measure the plasma parameters T, r_p and N, we must dump the plasma out of the trap against a microchannel plate-phosphor screen detector (MCP) (Peurrung & Fajans 1993). Since this operation destroys the plasma, only one of its properties is measured. Cycle-to-cycle reproducibility is therefore a basic assumption in this work. Using SDREVC we achieve $\mathrm{d}N/N < 1\,\%$ for any desired initial state.

To get T, the plasma is released slowly (∼1 ms). The flux of escaping particles is amplified by the MCP and generates a light signal on the phosphor screen. This signal, measured by a SiPM, is combined with the time-dependent confinement potential to reconstruct the tail of a Maxwellian (Eggleston *et al.* 1992). On a graph of log[SiPM signal] vs. −[confinement], the slope of the line that fits the rising edge is e/k_BT.

To get r_p or N, the plasma is released quickly (∼1 μs) using the high voltage pulser described above. The radial profile is captured by a CMOS camera (Thorlabs CS165MU1) and fit to a modified Gaussian (Evans 2016). To measure N, the back of the MCP is grounded, while the front (biased at +10 V) is connected to an integrator which produces a voltage $V = GNe/C$, where $G = 168$ is the amplifier gain and $C = 1.09$ nF is the combined capacitance of amplifier, cabling and parasitics.

The parameters L_p and n can be derived from r_p, N and the confining potentials. There exist several numerical plasma solvers for precise estimation of these quantities, but most of them assume that B is uniform; see for example Peinetti *et al.* (2006). Instead

https://doi.org/10.1017/S0022377823001022 Published online by Cambridge University Press

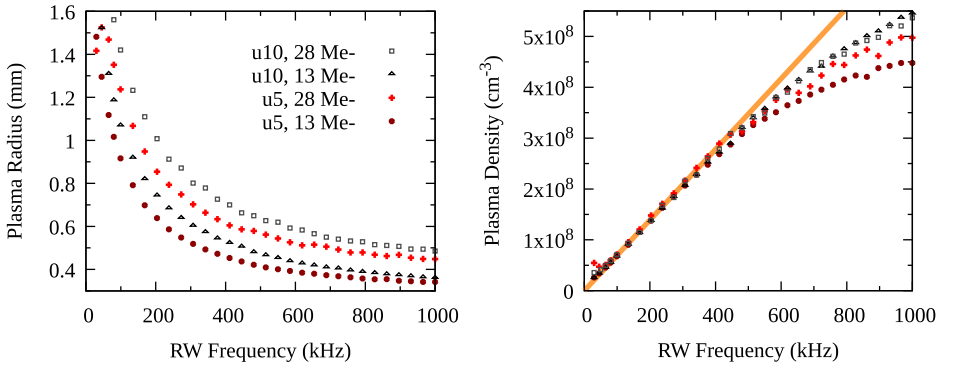

FIGURE 2. Control of the plasma density n using SDR in u5 and u10, for $N = 13 \times 10^6$ or $N = 28 \times 10^6$. Left: plasma radius r_p, measured as a function of applied RW frequency. Right: plasma density, evaluated as $n = N/(\pi r_p^2 L_p)$.

of developing a new code, here, we simply compute $n \approx N/\pi r_p^2 L_p$, where n and r_p, which actually vary with B, are understood to be an average over the length. In the limit $kT \ll e\phi_0$, L_p can be estimated as follows. We slowly release the plasma and record the on-axis potential difference between well bottom and barrier when the first particles begin to escape. This potential difference is approximately ϕ_0 at that instant. At the same instant, L_p is approximately the distance between the turning points of barely confined particles. To get from this to the plasma length during RW compression, we note that the product of L_p and ϕ_0 is roughly constant, i.e. $\phi_0 \propto N/L_p$ for a long plasma. The length of the fully confined plasma is then chosen from a table of L_p vs. $\phi_0 \times L_p$ for the appropriate well.

3. SDR

The RW technique is used to control r_p, and hence n (Huang *et al.* 1997). An electric dipole field with an amplitude of order 1V cm^{-1} revolves around the plasma in the plane perpendicular to B. The field presumably perturbs the radial edge of the plasma; it may also cause the centre of mass to oscillate (there is some speculation that the RW can recentre a plasma which began on a small diocotron orbit (A. P. Povilus, private communication 2014)). In the SDR, n evolves until the natural rotation rate of the plasma matches the RW frequency f (Danielson & Surko 2006).

In this regime, a graph of n vs. applied frequency f should be a line starting from the origin with slope $n/f = 4\pi\epsilon_0 B/e$, where ϵ_0 is the permittivity of free space (Ahmadi *et al.* 2018). Practically, we search for some combination of on-axis potential, RW amplitude and RW frequencies such that the linear relation is observed for the widest range of frequencies possible. Figure 2 shows examples from our experiment. The data are obtained by first preparing 13×10^6 or 28×10^6 electrons via SDREVC at 200 kHz in u5 (see figure 1*b*), then moving to another SDR well and compressing for 10 s at a different frequency f and higher RW amplitude (the RW waveforms are about 4 V_{pp} at the vacuum feedthrough). The SDR wells 'u5' and 'u10' are similar to those shown in figure 1(*b*).

Compression in u5 is linear up to approximately 400kHz; for u10 the range is slightly higher. In general, the useful range of SDR is less than 1 MHz for our experiment. A similar limit was found by Ahmadi *et al.* (2018). Danielson *et al.* (2007) suggested that SDR fails when the rotation rate is too close to one of the plasma's Trivelpiece–Gould modes, and that a stronger drive or a higher frequency can recover SDR in this case. However, we do not recover SDR for any frequency above 400 kHz. (Higher RW amplitude

https://doi.org/10.1017/S0022377823001022 Published online by Cambridge University Press

cannot be tested, but we do find that the amplitude can be decreased by a factor of 4 in u10 without changing the resulting radii.) We find that the steady-state T (while RW is still applied) increases monotonically with higher RW frequency, from 200 K at 500kHz to over 20 000 K at 3MHz. This may be a sign of increased expansion heating, which is expected at higher n, or else a symptom of phase slip between the drive and the plasma. A high-T failure mode would have been less relevant for Danielson *et al.* (2007), where $B = 4.8$ T, implying at least ten times faster cyclotron cooling in that experiment than in ours.

Within the range of frequencies where n is linear in f, we measure the same n for both test values $N = 13 \times 10^6$ and $N = 28 \times 10^6$. Accordingly, for higher N, r_p (and L_p) is relatively greater, while for greater L_p (u5 vs. u10), r_p is relatively smaller. These trends are clear from the data in figure 2. Thus, the data confirm our expectations for SDR compression. We conclude that the factor of two mirror field ratio does not compromise SDR in u5 or u10, nor does the use of a RW perturbation generated by three out of four 90° azimuthal sectors. No particles are lost, no halo is produced, no diocotron is induced and T is low (100–200 K) in both wells over the linear (SDR) range of RW frequencies.

We note, however, that our results do not reproduce the B dependence expected from the relation $n/f = 4\pi\epsilon_0 B/e$. First, the line in figure 2 has a slope corresponding to $B = 1$ T, which is a field value only reached at one extremity of the plasma; everywhere else the field is higher. Second, a given frequency should presumably give a denser plasma in u5 than in u10, because the average B in u10 is lower: $\langle B \rangle = 1.35$ T in u10 and 1.87T in u5. Yet the graph of $n$vs. f is nearly the same for both wells. The analysis may be compromised by other effects arising from the strong mirror field in the Cusp trap. A plasma spanning a large range of B should still reach a rigid-rotor equilibrium defined by a single rotation rate, but it is by no means cylindrical (Fajans 2003). A simple axial average $\langle B \rangle$ does not reflect the true distribution of particles, partly because of magnetic mirroring. Moreover, the assumption that particles follow the field lines does not hold for non-neutral plasma equilibrium in a magnetic mirror. This latter effect would tend to make the u5 plasma expand more than the u10 plasma during transfer to the pulsed dump well used for imaging, albeit only by a factor of 5 % if we use the first approximation given by Fajans (2003).

4. SDREVC

Starting with sufficiently many particles in any initial state, we use SDR to control n and EVC to control ϕ_0 (Ahmadi *et al.* 2018). Since n and ϕ_0 completely define the cold plasma equilibrium for a given well shape, this operation also fixes the remaining parameters L_p, r_p and N. In this section, we will first show that SDREVC, like SDR, works as well in u5 as in u10, with its strong gradient and one grounded RW sector. We then demonstrate a different, pulsed protocol, whereby ϕ_0 is reduced without EVC, resulting in the same level of reproducibility as standard SDREVC.

For this section we define 'any initial state' to be any one of five starting points prepared using SDREVC in u5. That is, we begin with SDREVC with the parameters given in one of the rows of table 1. Then we change wells, frequency and protocol for the final SDREVC to a fixed value.

4.1. *Standard Protocol*

We implement SDREVC by starting in an SDR well and slowly reducing the confinement. In order to maintain a constant amount of overlap with the RW electrode as the space charge decreases, we reduce both sides of the confining potential simultaneously. The starting point of this operation is shown in figure 1(*b*) for wells in u5 and u10. The excess charge is slowly released (EVC for 18 s) while n is locked by SDR at 200 kHz.

https://doi.org/10.1017/S0022377823001022 Published online by Cambridge University Press

RW freq. (kHz)	ϕ_0 (V)	N (10^6)	r_p (mm)
150	6.0	48.6	1.22
200	5.5	41.1	0.99
250	5.0	34.8	0.82
300	4.5	29.0	0.70
350	4.0	24.4	0.60

TABLE 1. Set of initial plasma preparations for testing different SDREVC routines.

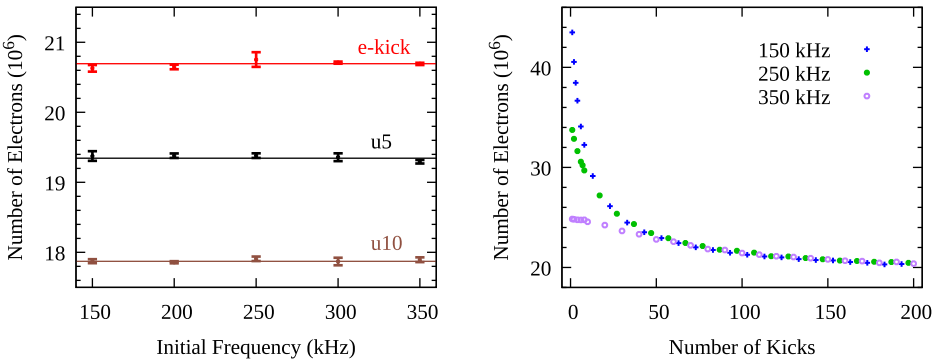

FIGURE 3. Control of the number of electrons using SDREVC and a variant with EVC replaced by e-kick. Left panel: reproducibilityof final number of electrons after SDREVC in u5 or u10 or the e-kick variant, for different initial plasma preparations (see table 1); data are reported as the mean of four measurements, with error bars showing ± 1 standard deviation. Right panel: convergence of the e-kick routine for three of these preparations; data points represent single measurements. The average number of electrons reported for the e-kick data set on the left is slightly higher (mean $= 20.7$ instead of 20.4) than the endpoint of the data on the right due to an unintended difference in the dump protocol (65 V instead of 100 V dump pulse).

The final number of electrons is plotted in figure 3 (left panel). Slightly different endpoints ($N = 17.9$ and 19.4×10^6) were chosen for the different SDREVC protocols so that the data would not overlap. The deviation from the endpoint value, as well as the standard deviation, is 1 % or less for any initial condition (1 % is one minor tick in the figure).

4.2. *Pulsed Protocol*

Instead of slowly reducing the confinement, we may use the pulsed electrode u13 to rapidly open and close the well such that only a fraction of the particles have time to escape. Such pulsing is sometimes referred to as an e-kick because electrons are thereby 'kicked out of' a mixed electron–antiproton plasma without losing the antiprotons. We use a 65 V, 50ns high voltage pulse to briefly switch from the 'closed' to 'open' configurations shown in figure 1(*c*). This is done once every 100 ms, which means the plasma is in the 'closed' well for 99.9999 % of the operation.

The routines used to obtain the data in the left panel of figure 3 employ 200 e-kicks, which amounts to 20s of RW compression and pulsing. The right panel shows the evolution of N as the number of e-kicks is varied. The convergence of different initial conditions to

https://doi.org/10.1017/S0022377823001022 Published online by Cambridge University Press

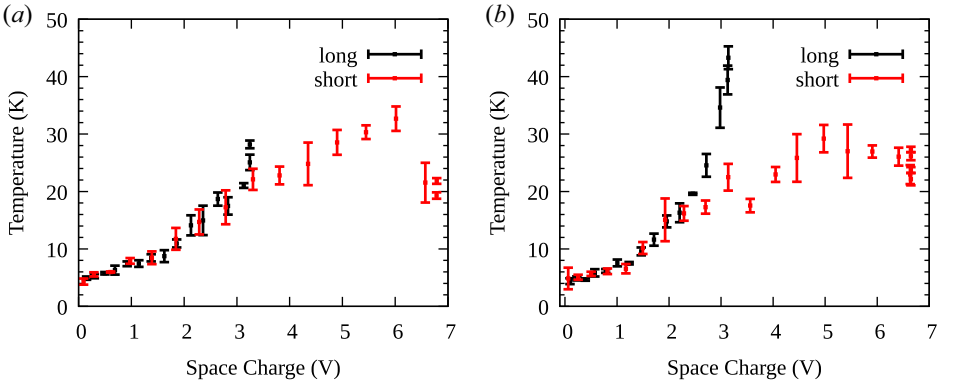

FIGURE 4. Evaporative cooling of electrons prepared with SDREVC at 150 kHz (*a*) or 350 kHz (*b*). Initial plasma parameters (rightmost points of each dataset) are $N = 19 \times 10^6$, $r_p = 0.72$mm (*a*) and $N = 16 \times 10^6$, $r_p = 0.45$ mm (*b*). The initial T is somewhat higher for the denser plasma in the long well.

a common (exponential) curve is faster than the exponential convergence of the entire set to a final, minimum value of N.

Immediately after turning off the RW, we measure $T = 170$ K for standard SDREVC in u5, 130 K for the same in u10, and 400K for the pulsed protocol. Not surprisingly, the e-kicked plasma is hotter. The ramp-shaped well shown in figure 1(*c*) gives better results with fewer e-kicks than a flat well. We assume this is either because the average B is higher (more cooling) than for a flat well spanning the same range in the axial direction, or because the ramp pushes the bulk of the plasma away from the high voltage pulses applied to u13 (less heating). Compression in the ramp-shaped well is not quite SDR; the graph of $n$vs. f is linear up to approximately 400kHz, but the intercept is slightly above the origin. This may also contribute to plasma heating. The high level of reproducibility obtained with the pulsed protocol is remarkable, given these apparent disadvantages.

5. EVC

Once the plasma has cooled to a low steady-state T, EVC is often used to reduce T further. However, forced EVC does not always lower T. In this section, we present data which suggest a link between ϕ_0 and the ultimate T achievable using EVC.

Figure 4 plots T as a function of ϕ_0 for plasma with the initial parameters given in the caption. The plasma is prepared with SDREVC, allowed to cool with the RW off for 10 s and then evaporatively cooled by reducing the confinement over 300ms. Different choices of final voltage on the rightmost potential barrier result in different final values of ϕ_0 and T. In this figure, data points and error bars represent the mean and standard deviation of 4 measurements; outliers were removed by starting with 5 measurements per bin and removing the one that deviated the most. 'Long' and 'short' refer to the well shapes shown in figure 1(*d*). The well bottom is at 50 V to improve the signal for the temperature diagnostic, which follows with as little manipulation as possible after EVC.

For $\phi_0 > 3$ V, EVC does not reduce T. For $\phi_0 < 3$ V, T is completely determined by the final value of ϕ_0. For example, if we want to EVC to $T < 15$ K, we must have $\phi_0 < 2$V. The value $\phi_0 = 2$ V corresponds to a range $4.5 < N < 15 \times 10^6$ and $0.3 < n < 1.2 \times 10^8$ cm^{-3} for the four datasets shown.

When N is reduced by EVC, r_p increases. The data for N and r_p (not shown) are well described by the relationship $Nr_p^2 = $ const., which is expected from the conservation of

https://doi.org/10.1017/S0022377823001022 Published online by Cambridge University Press

canonical angular momentum (O'Neil 1980). It follows that, for a given T, the highest n will be obtained by performing as little EVC as possible. According to our observations, this means reducing ϕ_0 as much as possible prior to EVC (while keeping the plasma compressed). In addition, since $\phi_0 \propto N/L_p$, more particles may be cooled to a given T by making the plasma longer.

6. Conclusion

This work offers some perspective on how far the SDR, EVC and SDREVC methods can be stretched to accommodate extreme or conflicting experimental requirements. In particular, it demonstrates that

(i) The SDR and SDREVC require neither a uniform magnetic field nor a pure dipole RW field. Equivalent performance is obtained in a strong mirror field using a RW with only three out of four sectors active.
(ii) The SDREVC-level reproducibility can be obtained using e-kick instead of EVC.
(iii) EVC to the lowest (reported) temperatures ($T \sim 10$ K) seems to require reducing the plasma space charge to $\phi_0 < 2$ V.

Item (i) shows that the simple theoretical argument given in Ahmadi *et al.* (2018) is experimentally robust. In principle, we might expect that any perturbation rotating in the correct direction should work on any plasma in rigid-rotor equilibrium. In practice, it is surprising that low T and high reproducibility are achieved in the presence of strong asymmetries in the azimuthal electric field (differing from pure dipole or quadrupole RW) and axial magnetic field. The only anomaly we observe is that the f vs. B relation expected for SDR is only valid here if we use the minimum value of B seen by the plasma. It is not clear to the authors why this value should be the relevant one.

Item (ii) may be worth considering for experiments where EVC is not reliable because of electronic noise; slowly opening the confining potential is equivalent to a downward sweep of the plasma bounce frequency, and noisy experiments may have trouble finding a frequency range without resonances. Another possible application comes from the particle-specific nature of the e-kick. So far, SDREVC has not been applied to antiprotons because they can only be compressed by the RW in the presence of electrons, which provide sympathetic cooling (Andresen *et al.* 2008; Aghion *et al.* 2018). In such a mixed plasma, it seems difficult to control whether electrons or antiprotons are removed by EVC. It is possible that some combination of standard SDREVC for electrons and pulsed SDREVC for the mixed electron–antiproton plasma could stabilize the final number of antiprotons in the presence of fluctuations in beam intensity from ELENA (Bartmann *et al.* 2018).

Item (iii) might be explained by analogy to the heating that occurs when the plasma expands radially: as electrons move to higher radii, ϕ_0 decreases and some of the potential energy of the electrons becomes kinetic energy. Similarly, one can imagine that kinetic energy is delivered to the plasma during EVC by the recoil from evaporating electrons. For sufficiently large ϕ_0, this hypothetical mechanism could even cause EVC to heat the plasma more than cool it, as is (marginally) suggested by the data for $\phi_0 > 5$ V. If the heating mechanism is as simple as this, then the seemingly arbitrary limit of $\phi_0 \approx 2$V may turn out to be fairly general. A similar process may account for some of the heating of antiprotons when the electrons are kicked out of a mixed electron–antiproton plasma, as suggested by Tietje (2022), although radial instabilities must also contribute to heating in this case.

https://doi.org/10.1017/S0022377823001022 Published online by Cambridge University Press

Acknowledgements

Editor Francesco Califano thanks the referees for their advice in evaluating this article.

Declaration of interest

The authors report no conflict of interest.

Funding

This work was supported by the Austrian Science Fund (FWF) Grant Nos. P 32468, W1252-N27, and P 34438; the JSPS KAKENHI Fostering Joint International Research Grant No. B 19KK0075; the Grant-in-Aid for Scientific Research Grant No. B 20H01930; Special Research Projects for Basic Science of RIKEN; Università di Brescia and Istituto Nazionale di Fisica Nucleare; and the European Union's Horizon 2020 research and innovation program under the Marie Sklodowska-Curie Grant Agreement No. 721559.

REFERENCES

Aghion, S., Amsler, C., Bonomi, G., Brusa, R.S., Caccia, M., Caravita, R., Castelli, F., Cerchiari, G., Comparat, D., Consolati, G., *et al.* 2018 Compression of a mixed antiproton and electron non-neutral plasma to high densities. *Eur. Phys. J.* D **72**, 1–11.

Ahmadi, M., Alves, B.X.R., Baker, C.J., Bertsche, W., Butler, E., Capra, A., Carruth, C., Cesar, C.L., Charlton, M., Cohen, S., *et al.* 2017 Antihydrogen accumulation for fundamental symmetry tests. *Nat. Commun*. **8** (1), 681.

Ahmadi, M., Alves, B.X.R., Baker, C.J., Bertsche, W., Capra, A., Carruth, C., Cesar, C.L., Charlton, M., Cohen, S., Collister, R., *et al.* 2018 Enhanced control and reproducibility of non-neutral plasmas. *Phys. Rev. Lett*. **120** (2), 025001.

Amsler, C., Antonello, M., Belov, A., Bonomi, G., Brusa, R.S., Caccia, M., Camper, A., Caravita, R., Castelli, F., Cheinet, P., *et al.* 2021 Pulsed production of antihydrogen. *Commun. Phys*. **4** (1), 19.

Amsler, C., Breuker, H., Chesnevskaya, S., Costantini, G., Ferragut, R., Giammarchi, M., Gligorova, A., Gosta, G., Higaki, H., Hunter, E.D., *et al.* 2022 Reducing the background temperature for cyclotron cooling in a cryogenic Penning–Malmberg trap. *Phys. Plasmas* **29** (8), 083303.

Andresen, G.B., Ashkezari, M.D., Baquero-Ruiz, M., Bertsche, W., Bowe, P.D., Butler, E., Cesar, C.L., Chapman, S., Charlton, M., Fajans, J., *et al.* 2010 Evaporative cooling of antiprotons to cryogenic temperatures. *Phys. Rev. Lett*. **105** (1), 013003.

Andresen, G.B., Bertsche, W., Bowe, P.D., Bray, C.C., Butler, E., Cesar, C.L., Chapman, S., Charlton, M., Fajans, J., Fujiwara, M.C., *et al.* 2008 Compression of antiproton clouds for antihydrogen trapping. *Phys. Rev. Lett*. **100** (20), 203401.

Aumann, T., Bartmann, W., Boine-Frankenheim, O., Bouvard, A., Broche, A., Butin, F., Calvet, D., Carbonell, J., Chiggiato, P., De Gersem, H., *et al.* 2022 Puma, antiproton unstable matter annihilation: Puma collaboration. *Eur. Phys. J.* A **58** (5), 88.

Bartmann, W., Belochitskii, P., Breuker, H., Butin, F., Carli, C., Eriksson, T., Oelert, W., Ostojic, R., Pasinelli, S. & Tranquille, G. 2018 The elena facility. *Phil. Trans. R. Soc.* A*: Math. Phys. Engng Sci*. **376** (2116), 20170266.

Blumer, P., Charlton, M., Chung, M., Clade, P., Comini, P., Crivelli, P., Dalkarov, O., Debu, P., Dodd, L., Douillet, A., *et al.* 2022 Positron accumulation in the gbar experiment. *Nucl. Instrum. Meth. Phys. Res. Sec.* A **1040**, 167263.

Chaney, A. & Sundararajan, R. 2004 Simple mosfet-based high-voltage nanosecond pulse circuit. *IEEE Trans. Plasma Sci*. **32** (5), 1919–1924.

Danielson, J.R. & Surko, C.M. 2006 Radial compression and torque-balanced steady states of single-component plasmas in penning-malmberg traps. *Phys. Plasmas* **13** (5).

Danielson, J.R., Surko, C.M. & O'Neil, T.M. 2007 High-density fixed point for radially compressed single-component plasmas. *Phys. Rev. Lett*. **99** (13), 135005.

EGGLESTON, D.L., DRISCOLL, C.F., BECK, B.R., HYATT, A.W. & MALMBERG, J.H. 1992 Parallel energy analyzer for pure electron plasma devices. *Phys. Fluids* B*: Plasma Phys*. **4** (10), 3432–3439.

EVANS, L.T. 2016 Phenomenology of creation of antihydrogen and measurement of antihydrogen properties. PhD thesis, University of California, Berkeley.

FAJANS, J. 2003 Non-neutral plasma equilibria, trapping, separatrices, and separatrix crossing in magnetic mirrors. *Phys. Plasmas* **10** (5), 1209–1214.

HORI, M. & WALZ, J. 2013 Physics at cern's antiproton decelerator. *Prog. Part. Nucl. Phys*. **72**, 206–253.

HUANG, X.-P., ANDEREGG, F., HOLLMANN, E.M., DRISCOLL, C.F. & O'NEIL, T.M. 1997 Steady-state confinement of non-neutral plasmas by rotating electric fields. *Phys. Rev. Lett*. **78** (5), 875.

HURST, N.C., DANIELSON, J.R., DUBIN, D.H.E. & SURKO, C.M. 2016 Evolution of a vortex in a strain flow. *Phys. Rev. Lett*. **117** (23), 235001.

KLUGE, H.-J., BEIER, T., BLAUM, K., DAHL, L., ELISEEV, S., HERFURTH, F., HOFMANN, B., KESTER, O., KOSZUDOWSKI, S., KOZHUHAROV, C., *et al.* 2008 Hitrap: a facility at gsi for highly charged ions. *Adv. Quant. Chem*. **53**, 83–98.

KURODA, N., TAJIMA, M., RADICS, B., DUPRÉ, P., NAGATA, Y., KAGA, C., KANAI, Y., LEALI, M., RIZZINI, E.L., MASCAGNA, V., *et al.* 2017 Antihydrogen synthesis in a double-cusp trap. In *Proceedings of the 12th International Conference on Low Energy Antiproton Physics (LEAP2016)*, 18, 011009.

MALMBERG, J.H. & DRISCOLL, C.F. 1980 Long-time containment of a pure electron plasma. *Phys. Rev. Lett*. **44** (10), 654.

NAGATA, Y., KANAI, Y., KURODA, N., HIGAKI, H., MATSUDA, Y. & YAMAZAKI, Y. 2015 The development of the superconducting double cusp magnet for intense antihydrogen beams. In *Journal of Physics: Conference Series*, vol. 635, p. 022062. IOP Publishing.

NAGATA, Y. & YAMAZAKI, Y. 2014 A novel property of anti-helmholz coils for in-coil syntheses of antihydrogen atoms: formation of a focused spin-polarized beam. *New J. Phys*. **16** (8), 083026.

NOTTE, J. & FAJANS, J. 1994 The effect of asymmetries on non-neutral plasma confinement time. *Phys. Plasmas* **1** (5), 1123–1127.

O'NEIL, T.M. 1980 A confinement theorem for nonneutral plasmas. *Phys. Fluids* **23** (11), 2216–2218.

PEINETTI, F., PEANO, F., COPPA, G. & WURTELE, J. 2006 Particle-in-cell method for parallel dynamics in magnetized electron plasmas: study of high-amplitude BGK modes. *J. Comput. Phys*. **218** (1), 102–122.

PEURRUNG, A.J. & FAJANS, J. 1993 A pulsed microchannel-plate-based non-neutral plasma imaging system. *Rev. Sci. Instrum*. **64** (1), 52–55.

SINGER, M., KÖNIG, S., STONEKING, M.R., STEINBRUNNER, P., DANIELSON, J.R., SCHWEIKHARD, L. & PEDERSEN, T.S. 2021 Non-neutral plasma manipulation techniques in development of a high-capacity positron trap. *Rev. Sci. Instrum*. **92** (12), 123504.

STENSON, E.V., NIßL, S., HERGENHAHN, U., HORN-STANJA, J., SINGER, M., SAITOH, H., PEDERSEN, T.S., DANIELSON, J.R., STONEKING, M.R., DICKMANN, M., *et al.* 2018 Lossless positron injection into a magnetic dipole trap. *Phys. Rev. Lett*. **121** (23), 235005.

TIETJE, I.C. 2022 Characterisation and control of antiproton-electron plasmas for pulsed antihydrogen production. PhD thesis, Technische Universität Berlin.

https://doi.org/10.1017/S0022377823001022 Published online by Cambridge University Press